Modeling the Friction Drilling Process Using a Thermo-Mechanical Coupled Smoothed Particle Galerkin Method

Cheng-Tang Wu, Youcai Wu, Wei Hu, and Xiaofei Pan

Abstract This paper presents an up-to-date Lagrangian particle method for the analysis of a coupled thermo-mechanical problem in the friction drilling simulation. The method is obtained by a modification of variational equations using the penalized approach to avoid onerous stability problems in conventional Lagrangian particle methods and to obtain semi-discrete equations that are amenable to temporal and spatial integration using the staggered explicit time marching scheme. To deal with the critical numerical limitation associated with large deformation and material separation at the bushing forming stage, the method is furnished with an adaptive anisotropic Lagrangian kernel and a bond-based failure criterion. Representative simulation of a thermal-mechanical coupled friction drilling process is studied, and results are compared with the experimental data to examine the validity of this study.

1 Introduction

Friction drilling is a nonconventional drilling process that utilizes the heat generated by friction between the rotating tool and metal workpiece to soften the material and create a hole [1]. Unlike traditional drilling, friction drilling is a chip-less and dry manufacturing method that produces the hole in only one operation without the material removal and lubricants. Friction drilling creates sturdy bushing on thin walled structures such as sheet metal or tubing. The bushing created in the process is usually two to three times thicker than the original workpiece allowing for mounting of soldered and screw connections in a simple and efficient way. Friction drilling can be performed on most metal materials using a high-speed rotating tool made of conical tungsten carbide. Typical applications of friction drilling in automotive industry include seat handle/frame, foot pedal, exhaust part, fuel rail, and among

C.-T. Wu (✉) · Y. Wu · W. Hu · X. Pan
Livermore Software Technology Corporation, Livermore, CA, USA
e-mail: ctwu@lstc.com

M. Griebel, M. A. Schweitzer (eds.), *Meshfree Methods for Partial Differential Equations IX*, Lecture Notes in Computational Science and Engineering 129,
https://doi.org/10.1007/978-3-030-15119-5_9

others. A growing interest on the study of friction drilling process has been shown by many car companies motivated by the need to reduce manufacturing costs and obtain the high quality of final product.

Numerical modeling is a necessary tool to understand the material flow, temperatures, stresses and strains which are difficult to measure experimentally during friction drilling [2]. Numerical simulation of friction drilling involves solving a coupled thermo-mechanical system, a task that can turn out to be difficult when considerable deformation and material separation are developed in bushing forming. It has become one of the research topics of great interest in computational mechanics over the last years. Since the Eulerian representation of a material has the difficulty to capture the free surface flow in the simulation of bushing forming, Lagrangian finite element methods [3] have been favored. While the Lagrangian finite element method is used in combination with the r-adaptive re-meshing strategy [4, 5] to handle large deformation problems in similar manufacturing processes such as the friction stir spot welding (FSSW) and the friction stir welding (FSW) [6, 7], modeling material separation in the friction drilling process has always been problematic. This is because the r-adaptive re-meshing may become unstable or unable to maintain the high quality mesh when some or lots elements are deleted using the element erosion technique in mimicking the material separation phenomenon during the forming of the metal bushing.

In comparison to Lagrangian finite element methods, Lagrangian particle methods are adventurous in modeling large deformation and material failure [8–10] problems. Lagrangian particle methods were also found to be very effective on reducing volumetric locking and shear locking in solid and structural analyses [11, 12]. Smoothed Particle Hydrodynamics (SPH) method developed by Gingold and Monaghan [13] and Lucy [14] in late 1970s for astrophysical problems has been considered the earliest Lagrangian particle method. In early 1990s, Libersky and Petschek [15] extended SPH to solid mechanics applications. In spite of its popularity in simulating high-velocity impact/penetration and fluid flow problems [16], SPH has limited success in solid mechanics applications due to several numerical instabilities. Among them, tensile instability [17], spurious zero-energy mode [18] and excessive straining [19] are critical to the simulation result and have been the important research topics in the past two decades.

Intensive research work has been carried out to resolve those numerical instabilities. For instance, the introduction of Lagrangian kernel [8, 20] or stress points method [21] has been proven to effectively remove the tension instability in Lagrangian particle methods. The origin of spurious zero-energy mode can be explained by inspecting the system of equations of the particle method. A pioneering approach to circumvent this numerical instability was demonstrated by Beissel and Belytschko [22] using a residual-type stabilization procedure. A variant of this stabilization approach includes the non-residual type of stabilization methods [23, 24], stabilized conforming nodal integration (SCNI) method [25], and variationally consistent integration methods [26]. The problem of excessive straining emerges as a numerical instability in Lagrangian particle methods when the strictly use of Lagrangian kernel is no more applicable in large deformation

range. In order to enable the Lagrangian kernel in large deformation analyses, semi-Lagrangian kernel [27] and adaptive anisotropic Lagrangian kernel [28] have been developed. Nevertheless, very few studies [24, 29] have addressed all numerical issues concurrently and comprehensively.

Smoothed Particle Galerkin (SPG) method motivated by Beissel and Belytschko's residual-type stabilization method [22] is one of the new Lagrangian particle methods developed by Wu et al. [29] to deal with those numerical instabilities. Another new Lagrangian particle method which is based on implicit gradient expansion [30], strain gradient stabilization technique [25] and semi-Lagrangian kernel [27] was proposed by Hillman and Chen [24] to sufficiently control those numerical instabilities in severe deformation analysis. These two Lagrangian particle methods share a common feature in augmenting the standard quadratic energy functional by a non-residual term for stabilization. Since the stabilization in those methods is accomplished without the use of the momentum equation residual, dependence of artificial control parameters for stabilization can be eliminated.

Modeling material separation in three-dimensional problem is another important research topic for Lagrangian particle methods as well as a desirable feature for industrial applications. However, the extant literature in Lagrangian particle methods gives very few examples [9] in simulating the three-dimensional material separation process. In essence, the development of 3D material separation techniques for Lagrangian particle methods face formidable challenges in tracing moving discontinuity surfaces and in dealing with the interaction of particles affecting by the discontinuity. In order to avoid those numerical difficulties and meet the current need in industrial applications, a bond-based failure criterion inspired by the peridynamics method of Silling et al. [31] was introduced to SPG method by Wu et al. [29] for material failure analysis. While the SPG method has been used to model ductile failure in metals recently [32], its application to the coupled thermo-mechanical problem in manufacturing applications remains to be developed.

The object of this study is to develop a thermo-mechanical coupled SPG method to realistically simulate the friction drilling process involving large deformation and material separation. The reminder of the paper is organized as follows: the preliminaries and weak formulations for the coupled thermo-mechanical problem are given in Sect. 2. In Sect. 3, the SPG formulation and semi-discrete equations are provided. The computational procedures for thermal and mechanical induced large deformation and material separation analyses are described in the Sect. 4. One friction drilling simulation using the present method is given in Sect. 5, and conclusions are made in Sect. 6.

2 Preliminaries

The highly coupled and nonlinear system in thermo-mechanical equations for the friction drilling simulation is usually difficult to be solved by the simultaneous time-stepping algorithm. In particular, the large and un-symmetric system in fully

coupled thermo-mechanical equations inevitably involves the convergent problem and is expensive to be solved implicitly in the presence of large deformation, material separation, severe contact conditions and contact-induced thermal shock. Additionally, because friction drilling is a very quick machining process, staggered and explicit time-stepping schemes are considered in this study for the application of interest. In the *staggered time-steeping algorithm* [33], the thermo-mechanical coupled system of equations is partitioned into a thermal phase at fixed configuration, followed by a mechanical phase at constant temperature.

In the thermal phase of the coupled system, we consider the transient heat transfer response of a metal workpiece in three-dimensional case. We assume linear dependence of heat flux on the temperature gradient which is known as the Fourier's law. We also assume isotropy of the material thermal conductivity. Since the temperature range over which the workpiece is observed in experiments is lower than the melting point, we presume the drilling process does not involve the material phase change. We also presume the heat generation is only due to plastic deformation and frictional contact between the drilling tool and workpiece. If we neglect the thermal exchange due to surface convection and radiation in the workpiece during the friction drilling, the standard variational formulation of the thermal energy conservation equation can be written to find the temperature field $\theta(X,t) \in \Theta = \{\theta \in H^1(\Omega) : \theta = \theta_d \text{ on } \partial\Omega_{\mathrm{d}}\}$ such that for arbitrary variation $\delta\theta \in \Theta_0 = \{\theta \in H^1(\Omega) : \theta = 0 \text{ on } \partial\Omega_d\}$ the following equation is satisfied

$$\begin{aligned}\int_{\Omega} \rho C_p \dot{\theta}\delta\theta \, d\Omega + \int_{\Omega} k\nabla\theta \cdot \nabla(\delta\theta)\, d\Omega = \int_{\partial\Omega_n} q_n \delta\theta \, ds + \int_{\Omega} Q\delta\theta \, d\Omega \\ + \int_{\partial\Omega_c} h_c(\theta - \theta_{\text{tool}})\delta\theta \, ds + \int_{\partial\Omega_c} \boldsymbol{\eta}\tau \cdot \left[\dot{u}^t\right]\delta\theta \, ds.\end{aligned} \tag{1}$$

In the above equation ρ is the mass density, C_p is the heat capacity, k is the isotropic thermal conductivity, ∇ is the gradient operator with respect to current position x, and "$\nabla\cdot$" denotes the divergence operator. $\partial\Omega_d$ describes a Dirichlet boundary imposed by a temperature θ_d, and $\partial\Omega_n$ is the Neumann boundary prescribed by a normal heat flux $q_n = k(\theta)\nabla\theta \cdot n$, where n is the outward unit normal vector. We also have Q denoting the internal heat generation rate per unit deformed volume from plastic deformation and is defined by

$$Q \coloneqq \eta S : \dot{\varepsilon}^p \tag{2}$$

where S and $\dot{\varepsilon}^p$ are the deviatoric part of Cauchy stress and the rate of plastic straining, respectively, and η is the Taylor-Quinney [34] coefficient that takes into account the fraction of heat generated by plastic deformation energy dissipation. The boundary $\partial\Omega_c$ denotes the contact surface with a thermal exchange between the tool and work piece. Subsequently, the third term on the right-hand side of Eq. (1) designates the interfacial heat transfer where h_c is the heat conductance on $\partial\Omega_c$, and

θ_{tool} is the temperature of the tool. The last term on the right-hand side of Eq. (1) represents the rate of frictional energy dissipation in which $\boldsymbol{\eta}$ is the fraction of heat generated by the frictional contact, and τ is the Cauchy contact traction and $\left[\dot{u}^t\right]$ is the contact slip rate which is regarded as the jump in velocity across contact surface.

In the mechanical phase, the dynamic process of friction drilling process is described by the equation of motion in the context of large strain analysis. During the friction drilling process, the workpiece experiences different rates of heating and cooling, and thus expansion and contraction. This leads to considerable thermal strains and stresses which need to be taken into account in the mechanical analysis. Using standard procedures, the variational equation for the mechanical problem in friction drilling process is written to find the displacement field $u(X,t) \in V = \{u \in H^1(\Omega) : u = u_g \text{ on } \partial\Omega_g\}$, such that for arbitrary variation $\delta u \in V_0 = \{u \in H^1(\Omega) : u = 0 \text{ on } \partial\Omega_g\}$, the following equation is satisfied:

$$\int_\Omega \rho\ddot{u} \cdot \delta u \, d\Omega + \int_\Omega \delta\left(\varepsilon(u)\right)^T : \sigma \, d\Omega = \int_\Omega b \cdot \delta u \, d\Omega + \int_{\Omega_h} h \cdot \delta u \, ds + \int_{\partial\Omega_c} \gamma \cdot \delta u \, ds \tag{3}$$

where b is the body force vector and σ is the Cauchy stress obtained from the constitutive law which is temperature dependent. The rate representation of strain field $\dot{\varepsilon}$ should consider the thermal effect which is described by

$$\dot{\varepsilon} = \dot{\varepsilon}^e + \dot{\varepsilon}^p + \dot{\varepsilon}^\theta \tag{4}$$

where $\dot{\varepsilon}^e$ is elastic strain rate tensor, and $\dot{\varepsilon}^\theta = \alpha\dot{\theta}$ is the thermal strain rate tensor with α denoting the thermal expansion coefficient. $\partial\Omega_g$ denotes a Dirichlet boundary imposed by a displacement u_g, and $\partial\Omega_h$ is the Neumann boundary prescribed by a surface traction h. γ denotes the contact traction which is governed by the unilateral contact conditions and Coulomb friction law [3]. Using Eq. (4) and the isothermal assumption from the staggered time-steeping algorithm, the corresponding rate form of the constitutive relation in mechanical phase can be written as

$$\dot{\sigma} = C(\theta) : \left(\dot{\varepsilon} - \dot{\varepsilon}^p - \dot{\varepsilon}^\theta\right) \tag{5}$$

where C is the temperature-dependent fourth-order isotropic elastic tensor.

Consequently, the thermal-mechanical problem in metal drilling process can be stated by coupling the mechanical weak form in Eq. (3) with the thermal weak form in Eq. (1) using the staggered time marching scheme. The coupled system of equations is discretized using meshfree approximations and solved by the classical explicit time-stepping approach which is described in the next section.

3 Particle Formulation

3.1 Meshfree Approximation and Discretization

The standard meshfree Galerkin method [8] for the thermal problem is formulated on a finite dimensional space $\Theta^s h \subset \Theta$ employing the thermal weak form of Eq. (1) to find $\theta^h(t) \in \Theta^h$ such that

$$\begin{aligned}\int_\Omega \rho C_p \dot{\theta}^h \delta\theta \, d\Omega + \int_\Omega k \nabla\theta^h \cdot \nabla\Big(\delta\theta^h\Big) \, d\Omega = \int_{\partial\Omega_n} q_n \delta\theta^h \, ds + \int_\Omega Q \delta\theta^h \, d\Omega \\ + \int_{\partial\Omega_c} h_c\Big(\theta^h - \theta_{\text{tool}}\Big)\delta\theta^h \, ds + \int_{\partial\Omega_c} \boldsymbol{\eta}\tau \cdot \Big[\dot{u}^t\Big]\delta\theta^h \, ds \quad \forall \delta\theta^h \in \Theta_0^h\end{aligned} \tag{6}$$

with initial condition

$$\theta^h(X, 0) = \theta_0(X) \quad \text{in } \Omega \tag{7}$$

where and $\Theta^h = \text{span}\{\phi_I^a : I \in Z_I\}$ and Z_I is an index set. $\{\phi_I^a\}_I \in Z_I$ are meshfree shape functions constructed by the meshfree convex approximation [35, 36] which is employed in this study to simplify the boundary condition enforcement.

For a particle distribution denoted by an index set $Z_I = \{X_I\}_{I=1}^{NP} \subset \mathbb{R}^3$, approximating the displacement field using the meshfree approximation gives

$$u^h(X, t) = \sum_{I \in Z_I} \phi_I^a(X) u(X_I, t) = \sum_{I \in Z_I} \phi_I^a \tilde{u}(t) \quad \forall X \in \Omega \tag{8}$$

where NP is the total number of particles in discretization. $\phi_I^a(X)$, $I = 1, \ldots, NP$ can be interpreted as Lagrangian shape functions of the meshfree approximation for the displacement field u^h as well as the temperature field θ^h where the superscript "a" denotes the support size of $\phi_I^a(X)$.

In order to prevent the tensile instability caused by the Eulerian kernel, the Lagrangian kernel approach [8] is considered in this development. Correspondingly, Eq. (6) is rewritten by

$$\begin{aligned}\int_\Omega \rho C_p \dot{\theta}^h \delta\theta \, d\Omega + \int_\Omega \Big(F^{-1} \cdot K \cdot F^{-T} \cdot \nabla^0\theta^h\Big) \cdot \nabla^0\Big(\delta\theta^h\Big) \, d\Omega = \int_{\partial\Omega_n} q_n \delta\theta^h \, ds \\ + \int_\Omega Q \delta\theta^h \, d\Omega + \int_{\partial\Omega_c} h_c\Big(\theta^h - \theta_{\text{tool}}\Big)\delta\theta^h \, ds + \int_{\partial\Omega_c} \boldsymbol{\eta}\tau \cdot \Big[\dot{u}^t\Big]\delta\theta^h \, ds \\ \forall \delta\theta^h \in \Theta_0^h\end{aligned} \tag{9}$$

where ∇^0 denotes the gradient operator with respect to reference position X, $K = kI^{(2)}$ is the thermal conductivity tensor with $I^{(2)}$ denoting the second-order identity tensor, and F is the deformation gradient. We remark that although the term *tensile instability* is reserved to describe the numerical instability of particle methods in structural analysis, we take the term in this paper to address the similar instability caused by the Eulerian kernel in the coupled thermo-mechanical analysis. Consequently, discrete points from meshfree discretization that carry the primary unknown variables are attached to the same set of material points throughout the course of deformation in Lagrangian particle methods. Under this consideration, the node set $Z_I = \{X_I,\ I = 1, \ldots, NP\}$ is the set of nodes defined in the reference configuration. In practice, the set of meshfree nodes can be taken from the finite element nodes created by a finite element mesh generator initially. Thus the geometrical representation of Ω can be numerically approximated by $\Omega \approx \bigcup_{I=1}^{NP} \Omega_I$ where Ω_I refers the volume of particle I which can be evaluated at time $t = 0$ using the information from the finite element mesh. The resultant discrete equations are then integrated using the direct nodal integration (DNI) scheme.

We can also formulate the mechanical weak form of Eq. (3) in similar fashion. Nevertheless, an application of the DNI scheme to Lagrangian particle methods leads to another numerical instability known as the zero-energy mode in structural analysis. To suppress the zero-energy mode and stabilize the solution for friction drilling simulation, the standard smoothed particle Galerkin (SPG) method [28, 29] is employed with a consideration of the thermal effect. The essence of SPG method in structural analysis is to augment the standard energy functional by a stabilization term using the penalty approach. As opposed to the residual-type stabilization method [22] which uses the residual of the momentum equation and artificial control parameters to effect stabilization, SPG method introduces a projection of displacement gradients on to a strain space leading to an additional term that penalizes the difference in strain fields for stabilization. The penalty approach modifies the DNI scheme and gives rise to a dual stress-points algorithm [28] which can be easily implemented and parallelized for the large-scale computation in industrial applications. The reader is refer to [28, 29] for detail information and references on SPG method. The SPG method for mechanical part of the coupling problem we considered is then as follows: find $u^h(X, t) \in V^h$ such that

$$\int_\Omega \rho \ddot{u}^h \cdot \delta u^h \, d\Omega + \underbrace{\int_\Omega \sigma : \left(F^{-1} \cdot \nabla^0 \delta u^h \right) d\Omega}_{\text{standard}} + \underbrace{\int_\Omega \delta \left(F^{-1} \cdot \nabla^0 \left(F^{-1} \cdot \nabla^0 \delta u^h \right) \cdot \lambda \right)^T : \tilde{\sigma} \, d\Omega}_{\text{stabilization}}$$
$$= \int_\Omega b \cdot \delta u^h \, d\Omega + \int_{\Omega_n} h \cdot \delta u^h \, ds + \int_{\partial\Omega_c} \gamma \cdot \delta u^h \, ds \quad \forall \delta u^H \in V_0^h \tag{10}$$

with initial conditions

$$u^h(X,0) = u_0(X) \tag{11}$$

$$\dot{u}^h(X,0) = \dot{u}_0(X) \tag{12}$$

where the stabilization term is composed of first-order strain gradients, stabilization stresses $\tilde{\sigma}$, and stabilization coefficient matrix $\lambda(x)$ that can be found in [28, 29].

3.2 Semi-discrete Equations

The semi-discrete equations of the thermal problem can be expressed by the following algebraic equations.

$$\tilde{\theta} + \mathbf{H}\tilde{\theta} = \mathbf{P} \tag{13}$$

where

$$C_{IJ} = \int_{\Omega_x} \rho_0 C_p \Psi_I \Psi_J \, d\Omega_X \tag{14}$$

$$H_{IJ} = \int_{\Omega} k F_{il}^{-1} F_{lj}^{-T} \Psi_{I,j} \Psi_{J,i} \, d\Omega + \int_{\partial\Omega_c} h_c \Psi_I \Psi_J \, ds \tag{15}$$

$$P_I = \int_{\Omega} \eta S : \dot{\varepsilon}^p \Psi_I \, d\Omega + \int_{\partial\Omega_n} q_n \Psi_I \, ds + \int_{\partial\Omega_c} \left(h_c \theta_{\text{tool}} - \boldsymbol{\eta}\tau \cdot \left[\dot{u}^t \right] \right) \Psi_I \, ds \tag{16}$$

Thermal equation in Eq. (13) is marched through time using the forward difference algorithm [3] which is given by

$$\tilde{\theta}_{n+1} = \tilde{\theta}_n + \Delta t \dot{\tilde{\theta}}_n \tag{17}$$

$$\dot{\tilde{\theta}}_n = C^{l\,-1} \left(P_n - H_N \tilde{\theta}_n \right) \tag{18}$$

where the thermal capacity matrix C is advantageously replaced by the lumped matrix C^l for the explicit analysis. When the tool surface is in contact with the workpiece, the standard Fourier's law cannot be used to fully describe the heat transfer phenomena because the contact surfaces do not physically match perfectly. In this case, the heat resistance generally decreases as contact pressure increases. For this reason, the heat conductance h^c in the thermal contact is assumed to be a

function of normal contact pressure, thermal conductivity of the gas, yielding stress of the work piece and surface roughness as described in [37].

In a similar way, the semi-discrete equations of the mechanical problem are given by

$$M\ddot{\tilde{U}} = F^{\text{ext}} + F^{c} - F^{\text{int}} - F^{\text{stab}} \tag{19}$$

where the mass matrix M, external force F^{ext}, internal force F^{int}, and stabilization force F^{stab} for the SPG method can be found in [28, 29, 32]. F^{c} is the contact force which is given by

$$F_I^c = \int_{\partial\Omega_c} \gamma \phi_I^a \, ds \tag{20}$$

Since the tungsten carbide tool is also meshed by the finite element discretization, the mechanical contact between the workpiece and drilling tool is modelled using the standard node-to-surface penalty contact algorithm [3, 38].

It also suffices to integrate Eq. (19) by the central difference integration algorithm and results in

$$\dot{\tilde{U}}_{n+1/2} = \dot{\tilde{U}}_{n-1/2} + \frac{\Delta t_{n+1} + \Delta t_n}{2} \ddot{\tilde{U}}_n \tag{21}$$

$$\dot{\tilde{U}}_{n+1} = \tilde{U}_n + \Delta t_{n+1} \ddot{\tilde{U}}_{n+1/2} \tag{22}$$

$$\ddot{\tilde{U}}_n = M^{l\,-1} \left(F_n^{\text{ext}} + F_n^{c} - F_n^{\text{int}} - F_n^{\text{stab}} \right) \tag{23}$$

where M^l is the lumped mass matrix. Noting that the temperature remains constant and material properties are temperature dependent during this mechanical phase.

The critical time step in the explicit method is governed by the Courant-Friedrichs-Lewy (CFL) condition [3] which is given in the following for the thermal and mechanical analysis respectively

$$\Delta t^{\theta} \leq S_c \min \left(\frac{\rho C_p l^2}{2k} \right), \quad \Delta t^{u} \leq S_c \min \left(\frac{l}{C_u} \right) \tag{24}$$

where the sound speed C_u gives the characteristic speed of the medium in mechanical analysis. l is the support size of the kernel [8] for the particle system. A scaling factor $S_c = 0.15$ is used in this study.

4 Large Deformation and Material Separation Analyses

In this section, we discuss the computational procedures of the present method for the analysis of large deformation and material separation problems in frictional drilling simulation.

4.1 The Adaptive Anisotropic Lagrangian Kernel for Large Deformation Analysis

As mentioned earlier in the Introduction, Lagrangian kernel has been utilized in the particle method to remove the tension instability in the nonlinear structural analysis. However, the Lagrangian particle methods experience the excessive straining problem when the strictly use of Lagrangian kernel is no more applicable. Specifically, the excessive straining during the large deformation friction drilling simulation inevitably causes the numerical breakdown when the deformation gradient computed at the particle ceases to become invertible.

In order to handle the excessive straining problem, an adaptive anisotropic Lagrangian kernel is considered [28]. Using the chain rule, the calculation for the deformation gradient at the particle can be rewritten [32] as

$$F^{n+m} = \widehat{F}^{n+m} F^{n} \tag{25}$$

where $\widehat{F}^{n+m}(\widehat{x})$ is the decomposed deformation gradient, from $t = t_n$ to t_{n+m}, computed based on the new reference configuration and is given by

$$\begin{aligned} \widehat{F}_{ij}^{n+m}(X_J) = & \quad \frac{\partial \widehat{x}_i}{\partial \widehat{X}_j} = \sum_{I=1}^{NP} \frac{\partial \phi_I^a(\widehat{X}_J)}{\partial \widehat{X}_j} \widehat{x}_{iI}(X, t_{n+m}) \\ = & \sum_{I=1}^{NP} \frac{\partial \phi_I^a(\widehat{X}_J)}{\partial \widehat{X}_j} \left(\widehat{X}_{iI} + \tilde{u}_{iI}(X, t_{n+m}) \right) \\ = & \quad \delta_{ij} + \sum_{I=1}^{NP} \frac{\partial \phi_I^a(\widehat{X}_J)}{\partial \widehat{X}_j} \tilde{u}_{iI}(X, t_{n+m}) \end{aligned} \tag{26}$$

Here, $\widehat{x} = \widehat{X} + \tilde{u}(X, t_{n+m})$ is a position vector defined in the new reference configuration $\widehat{X}=x(X,t_n)$. A local $\widehat{X}^I$-coordinate system in which the axes are parallel to the global Cartesian coordinates and the origin is located at $\widehat{X}_I$ which is defined for each particle I. In each new reference configuration, an ellipsoidal nodal support is defined for the neighbor particle searching. The three-dimensional ellipsoidal cubic

spline kernel function is defined in another local $\widehat{\widehat{x}}^I$-coordinate system by

$$\varphi_I^a(\widehat{X}_J) = \varphi_1\left(\frac{\widehat{\widehat{X}}_J^I}{h_1^n}\right)\varphi_1\left(\frac{\widehat{\widehat{Y}}_J^I}{h_2^n}\right)\varphi_1\left(\frac{\widehat{\widehat{Z}}_J^I}{h_3^n}\right) \tag{27}$$

where ϕ_1 is a standard one-dimensional cubic spline kernel function, h_1^n, h_2^n and h_3^n are the current semi-major axes of the ellipsoid. The sizes of semi-major axes can be considered the support sizes of the kernel and are updated according to the deformation [28]. $\widehat{\widehat{X}}_J^I$, $\widehat{\widehat{Y}}_J^I$ and $\widehat{\widehat{Z}}_J^I$ are the projections of relative position vector $\widehat{X}_J - \widehat{X}_I$ on the local $\widehat{\widehat{x}}^I$-coordinate system respectively. The adaptive anisotropic Lagrangian kernel is updated constantly over a period of time. The spherical shape domain of cubic spline kernel function deforms and rotates according to the Lagrangian motion between each two adaptive Lagrangian kernel steps. We address the reader to reference [28] for a comprehensive description of the approach. For the computational efficiency in explicit time integration method, the material derivatives of meshfree shape functions are always computed and stored at the new reference configuration and reused during the time stepping.

Since the operation of adaptive anisotropic Lagrangian kernel does not involve remeshing, the stress-recovery techniques or remapping procedures are not necessary. This unique property of present method leads to a relatively simple mathematical formulation for simulating the large strain problems.

4.2 The Bond-Based Failure Criterion for Material Separation Analysis

Excessive straining also appears in the friction drilling process when the material of workpiece starts to fail at the bushing forming stage. Precisely, the C^1-continuity assumption in Lagrangian particle methods is inadequate to describe the kinematic discontinuity of displacement field in a continuous setting for the failure analysis [19]. This makes Lagrangian particle methods even more challenging in friction drilling simulation.

To further avoid the excessive straining problem due to the assumption of continuous displacement field in the friction drilling simulation, a bond-based failure criterion [29, 31] is incorporated with the present coupled thermal-mechanical formulations. The origins of this approach can be traced back to the bond failure in peridynamics [31, 39] in which material failure is modeled through bond breakage. In Lagrangian particle methods, the bond is a representation of a connection between two particles. Given a length of the bond $\|X_J - X_I\|$ for a particle pair consisting of particles I and J in the initial configuration, the stretch ratio e_{IJ} of the bond is defined by

$$e_{IJ} = \frac{\|x_J - x_I\|}{\|X_J - X_I\|} \tag{28}$$

For the friction drilling simulation, we restrict our attention to the material failure in metals. In the bond-based failure criterion for ductile material, two neighbor particles are considered disconnected during the neighbor particle sorting whenever their averaged effective plastic strain and stretch ratio reach their respective critical values. Accordingly, the three-dimensional ellipsoidal cubic spline kernel function in Eq. (27) for a pair of particles I and J can be modified as:

$$\phi_I^a\left(\widehat{X}_J\right) = \begin{cases} 0, & \text{if } \widehat{X}_J \notin \operatorname{supp}\left(\phi_I^a\right) \\ & \text{or } \left(\bar{\varepsilon}_{IJ}^P > \bar{\varepsilon}_{\text{crit}}^p \text{ and } e_{IJ} > e_{\text{crit}}\right) \\ \phi_1\left(\frac{\hat{\bar{X}}_J^I}{h_1^n}\right)\phi_1\left(\frac{\hat{\bar{Y}}_J^I}{h_2^n}\right)\phi_1\left(\frac{\hat{\bar{Z}}_J^I}{h_3^n}\right), & \text{otherwise} \end{cases} \tag{29}$$

where $\bar{\varepsilon}_{ij}^p = \left(\bar{\varepsilon}^p\left(\widehat{X}_J\right)\right)/2$, and $\bar{\varepsilon}^p$ denoting the effective plastic strain. $\bar{\varepsilon}_{\text{crit}}^p$is the critical effective plastic strain for bond failure, and e_{crit} denotes the critical stretch ratio. We consider $e_{\text{crit}} \geq 1.0$ in our numerical analysis which implies that the bond failure does not occur under compression. This implication is valid for most metal failure process.

Because the effective plastic strain at each particle is monotonically increasing during the course of deformation, the kinematic disconnection in a particle pair is considered as a permanent and irreversible process. This is a substantial characteristic for the present method in metal failure analyses since the non-physical material self-healing and excessive straining issues can also be completely excluded from the material failure simulation.

5 Numerical Example

A friction drilling process of AISI 304 stainless steel is modeled and compared with the experimental data in this section. The normalized nodal support size of 1.9 is used and the adaptive anisotropic Lagrangian kernel is updated every 50 time steps in the explicit dynamic analysis.

The AISI 304 stainless steel specimen used in the friction drilling process has a diameter of 18 mm and thickness of 1.5 mm [40]. The geometry of the tool is shown in Fig. 1a. The tool, which rotates at 3000 rpm and plunges at 100 mm/min in the test, is modeled by rigid material and meshed using tetrahedral finite elements. As can be seen in Fig. 1b, the metal workpiece is discretized using 12,607 Lagrangian particles. Finer discretization with a nodal distance of approximately 0.25 mm is employed in the central portion of the specimen where large deformation and material separation occurs. As such, the explicit time step size for thermal analysis is 50 µs and for structural analysis is about 4 µs. The perimeter of the workpiece is clamped. The stress flow in the AISI 304 steel is modeled by the Johnson-Cook material law [41] (parameters: $A = 205$ MPa, $B = 802.5$ MPa, $C = 0.08$, $m =$

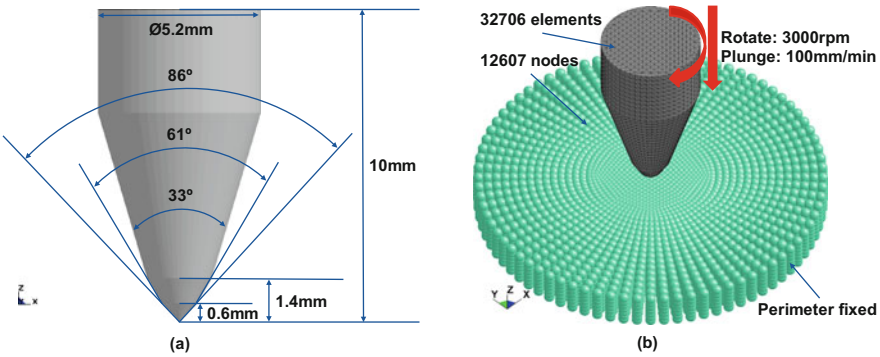

Fig. 1 Friction drilling: (**a**) tool geometry, (**b**) discretization and boundary conditions

1.09, $n = 0.622$). The failure behavior of the steel is handled by the SPG bond failure mechanism as described in Sect. 4.2 rather than the Johnson-Cook damage law, and the effective plastic strain for bond failure is set to 0.4. According to efunda (www.efunda.com), the Young's modulus of the workpiece is set to 193 GPa. The thermal properties of the AISI stainless steel are: coefficient of thermal expansion 0.0000184, heat capacity C_p 500 J/kg-K, and thermal conductivity k 16.2 W/m-K. The coefficient of friction (COF) between the tool and the workpiece is set to 0.2 for the node-to-surface contact algorithm in the numerical analysis. The fraction of heat generation $\boldsymbol{\eta}$ in the frictional contact is taken to be 0.5. The interfacial heat transfer between the tool and the workpiece is neglected. The Taylor-Quinney [34] coefficient η of 0.9 is considered in Eq. (2).

The comparison of thrust force and torque is presented in Fig. 2a and b, respectively. Both the force and torque responses capture the basic profiles of experimental data nicely. Further improvement in the force and torque results can be made by tuning the coefficient of contact friction. But this is not within the scope of this study and therefore not considered in this numerical example.

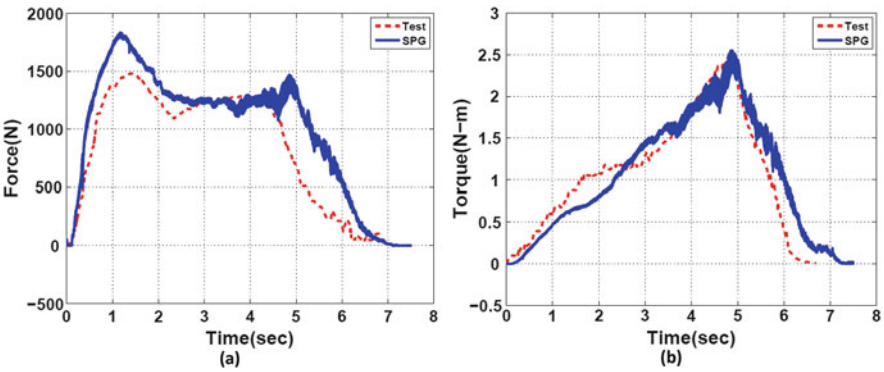

Fig. 2 Response of friction drilling: (**a**) thrust force, (**b**) torque

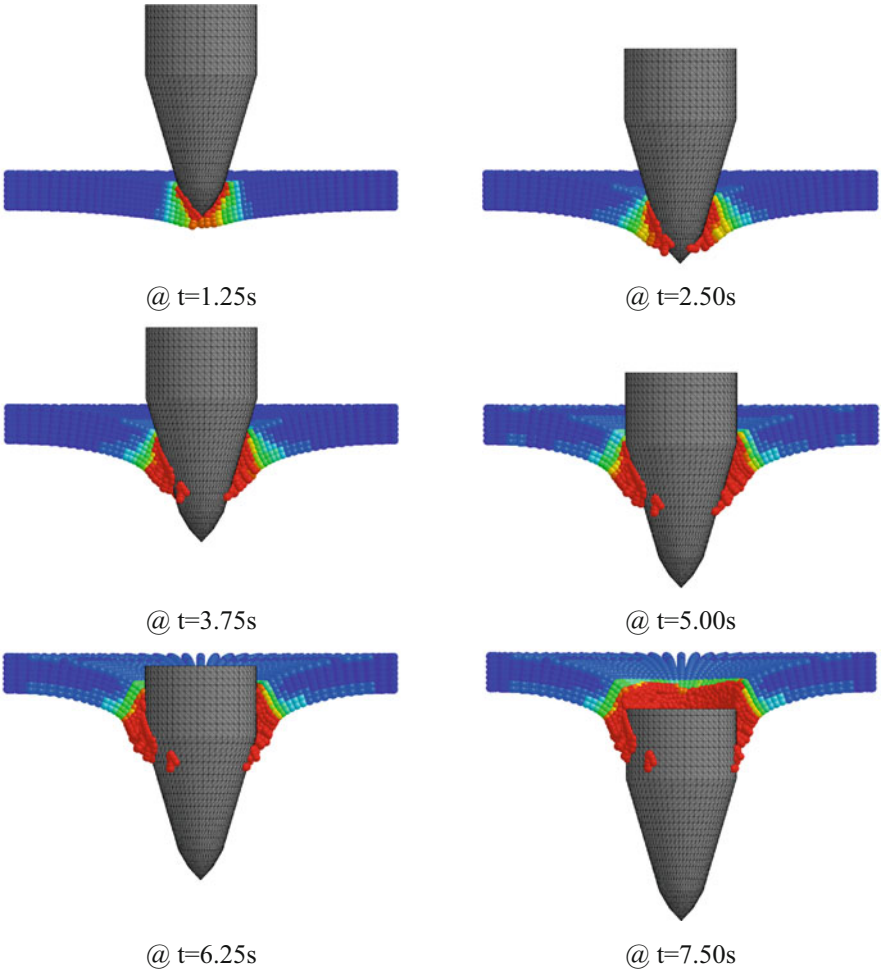

Fig. 3 Friction drilling: effective plastic strain distribution (red $\geq$ 0.4, blue: 0)

Figure 3 shows the evolution of the effective plastic strain in the workpiece while only half of it is plotted. Red color indicates effective plastic strain level of 0.4 (which is the bond failure criterion) or more. It should be pointed out that bond failure, i.e., material separation, only occurs when the effective plastic strain and stretch ratio both reach their respective critical values. As shown in Fig. 3, material failure occurs in a relatively small region and the bushing is qualitatively formed. It is worthwhile to emphasize that the creation of bushing shape is one of the major purposes of this type manufacturing process. However, it is not captured by any other numerical technique by far.

Figure 4 shows the simulation result of temperature distribution during the friction drilling process (back view). Red color indicates temperature rising of

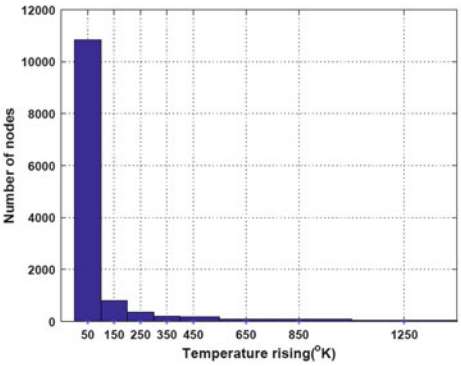

Temperature statistics

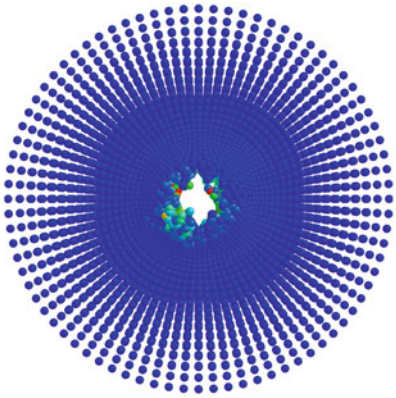

@ t=2.50 sec

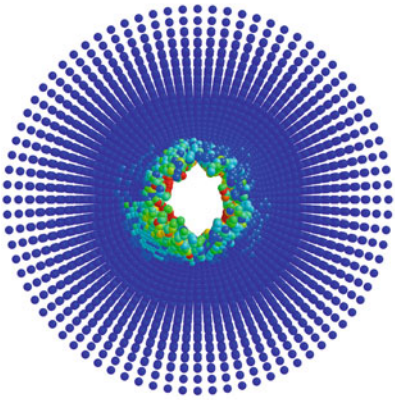

@ t=3.75 sec

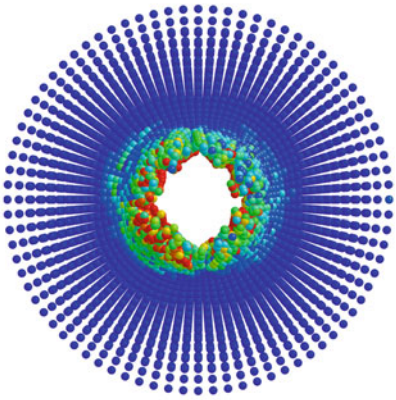

@ t=5.00 sec

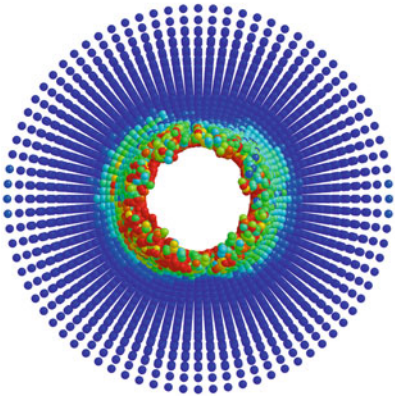

@ t=6.25 sec

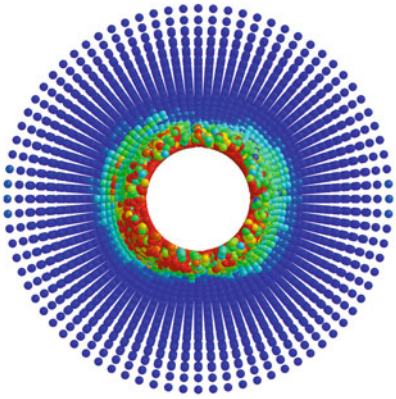

@ t=7.50 sec

Fig. 4 Friction drilling: temperature field in workpiece (red: $\geq 100°$K, blue: $0°$K)

100°K or more, and blue color means no temperature rising. Due to the low thermal conductivity in AISI 304 stainless steel, the temperature rising is less than 100°K for more than 90% of the particles. Very few particles (about 1%) directly in contact with the tool have a temperature rising to 800°K or more. The simulation result is close to the measured temperature on the upper side of the disc at the contact zone which was reported at 842°K [40]. The heat wave did not propagate far away from the tool-workpiece contact region because of the low thermal conductivity of the workpiece and the fast machining process.

6 Conclusions

The main difficulty in finite element modeling of friction drilling process consists in dealing with high levels of deformations involving in the complex material flow due to frictional heating and material separation at the busing forming stage. Despite the enormous progress achieved lately in computational mechanics, the development of an advanced numerical tool for the robust and accurate friction drilling simulation continues to be nowadays an emerging need for industry.

In this study, we have introduced a Lagrangian particle method that is suitable for the three-dimensional thermo-mechanical analysis and can become a promising alternative numerical tool for the friction drilling simulation. The present method is developed to improve several numerical instabilities in conventional Lagrangian particle methods. The numerical results in this study suggest that the present method is able to produce the desired physics in the forming of a busing and generate reasonable force and torque responses compared with the experimental data. To the authors' best knowledge, the existing literature has not been able to demonstrate similar results. The extension of this method to other thermo-mechanical problems that consider complex multi-physics behaviors such as phase transformation and phase change will be the focus of our future development.

Acknowledgements The authors wish to thank Dr. John O. Hallquist of LSTC for his support to this research. The support from Ford Motor Company is also gratefully acknowledged.

References

1. S.F. Miller, A.J. Shih, P.J. Blau, Microstructural alterations associated with friction drilling of steel, aluminum, and titanium. J. Mater. Eng. Perform. **15**, 647–653 (2005)
2. S.F. Miller, A.J. Shih, Thermo-mechanical finite element modeling of the friction drilling process. J. Manuf. Sci. Eng. **129**, 531–538 (2007)
3. T. Belytschko, W.K. Liu, B. Moran, K.I. Elkhodary, *Nonlinear Finite Elements for Continua and Structures*, 2nd edn. (Wiley, Chichester, 2014)
4. B. Padma Raju, M. Kumara Swamy, Finite element simulation of a friction drilling procedure using Deform-3D. Int. J. Eng. Res. Tech. **2**, 716–721 (2012)

5. A. Gopichand, M. Veera Brahmam, D. Bhanuprakash, Numerical simulation and analysis of friction drilling process for aluminum alloy using Ansys. Int. J. Eng. Res. Tech. **3**, 602–607 (2014)
6. G. Buffa, J. Hua, R. Shivpuri, L. Fratini, A continuum based FEM model for friction stir welding – model development. Mater. Sci. Eng. A **419**, 389–396 (2006)
7. B. Meyghani, M.B. Awang, S.S. Emamian, M.K.B. Mohd Nor, S.R. Pedapati, A comparison of different finite element methods in the thermal analysis of friction stir welding (FSW). Metals **10**, 450 (2017)
8. J.S. Chen, C. Pan, C.T. Wu, W.K. Liu, Reproducing kernel particle methods for large deformation analysis of non-linear structures. Comput. Methods Appl. Mech. Eng. **139**, 195–227 (1996)
9. T. Rabczuk, T. Belytschko, Cracking particles: a simplified meshfree method for arbitrary evolving cracks. Int. J. Numer. Methods Eng. **61**, 2316–2343 (2004)
10. D.C. Simkins, S. Li, Meshfree simulation of thermo-mechanical ductile fracture. Comput. Mech. **38**, 235–249 (2006)
11. S. Li, W. K. Liu, *Meshfree Particle Method* (Springer, Berlin, 2004)
12. D.D. Wang, J.S. Chen, Locking free stabilized conforming nodal integration for meshfree Mindlin-Reissner plate formulation. Comput. Methods Appl. Mech. Eng. **193**, 1065–1083 (2004)
13. R.A. Gingold, J.J. Monaghan, Smoothed particle hydrodynamics – theory and application to non-spherical stars. Mon. Not. R. Astron. Soc. **181**, 375–389 (1977)
14. L.B. Lucy, A numerical approach to the testing of the fission hypothesis. Astron. J. **82**, 1013–1024 (1977)
15. L.D. Libersky, A.G. Petschek, Smooth particle hydrodynamics with strength of materials. Lect. Notes Phys. **395**, 248–257 (1990)
16. M.S. Shadloo, G. Oger, D.L. Touzé, Smoothed particle hydrodynamics method for fluid flows, towards industrial applications: motivations, current state, and challenges. Comput. Fluid **136**, 11–34 (2016)
17. W. Swegle, D.L. Hicks, S.W. Attaway, Smoothed particle hydrodynamics stability analysis, Comput. Mech. **116**, 123–134 (1995)
18. T. Belytschko, Y. Guo, W.K. Liu, S.P. Xiao, A unified stability analysis of meshless particle methods. Int. J. Numer. Methods Eng. **48**, 1359–1400 (2000)
19. C.T. Wu, N. Ma, K. Takada, H. Okada, A meshfree continuous-discontinuous approach for the ductile fracture modeling in explicit dynamics analysis. Comput. Mech. **58**, 391–409 (2016)
20. T. Rabczuk, T. Belytschko, S.P. Xiao, Stable particle methods based on Lagrangian kernels. Comput. Methods Appl. Mech. Eng. **193**, 1035–1063 (2004)
21. C.T. Dyka, P.W. Randles, R.P. Ingel, Stress points for tension instability in SPH. Int. J. Numer. Methods Eng. **40**, 2325–2341 (1997)
22. S. Beissel, T. Belytschko, Nodal integration of the element-free Galerkin method. Comput. Methods Appl. Mech. Eng. **139**, 49–74 (1996)
23. C.T. Wu, M. Koishi, W. Hu, A displacement smoothing induced strain gradient stabilization for the meshfree Galerkin nodal integration method. Comput. Mech. **56**, 19–37 (2015)
24. M. Hillman, J.S Chen, An accelerated, convergent, and stable nodal integration in Galerkin meshfree methods for linear and nonlinear mechanics. Int. J. Numer. Methods Eng. **107**, 603–630 (2016)
25. J.S. Chen, C.T. Wu, S. Yoon, Y. You, A stabilized conforming nodal integration for Galerkin Meshfree methods. Int. J. Numer. Methods Eng. **50**, 435–466 (2001)
26. M. Hillman, J.S. Chen, S.W. Chi, Stabilized and variationally consistent nodal integration for meshfree modeling of impact problems. Comput. Part. Mech. **1** 245–256 (2014)
27. P.C. Guan, J.S. Chen, Y. Wu, H. Tang, J. Gaidos, K. Hofstetter, M. Alsaleh, Semi-Lagrangian reproducing kernel formulation and application to modeling earth moving operations. Mech. Mater. **41**, 670–683 (2009)

28. C.T. Wu, S.W. Chi, M. Koishi, Y. Wu, Strain gradient stabilization with dual stress points for the meshfree nodal integration method in inelastic analysis. Int. J. Numer. Methods Eng. **107**, 3–30 (2016)
29. C.T. Wu, Y. Wu, J.E. Crawford, J.M. Magallanes, Three-dimensional concrete impact and penetration simulations using the smoothed particle Galerkin method. Int. J. Impact Eng. **106**, 1–17 (2017)
30. J.S. Chen, X. Zhang, T. Belytschko, An implicit gradient model by a reproducing kernel strain regularization in strain localization problems. Comput. Methods Appl. Mech. Eng. **193**, 2827–2844 (2014)
31. S.A. Silling, E. Askari, A meshfree method based on the peridynamic model of solid mechanics. Comput. Struct. **83**, 1526–1535 (2005)
32. C.T. Wu, T.Q. Bui, Y.C. Wu, T. L. Luo, M. Wang, C.C. Liao, P.Y. Chen, Y.S. Lai, Numerical and experimental validation of a particle Gakerkin method for metal grinding simulation. Comput. Mech. **61**(3), 365–383 (2018). https://doi.org/10.1007/s00466-017-1456-6
33. C.A. Felippa, K.C. Park, Staggered transient analysis procedures for coupled dynamic systems. Comput. Methods Appl. Mech. Eng. **26**, 61–112 (1980)
34. T. J. R. Hughes, *The Finite Element Method* (Prentice-Hall, Englewood Cliffs, 2000)
35. C.T. Wu, C.K. Park, J.S. Chen, A generalized approximation for the meshfree analysis of solids. Int. J. Numer. Methods Eng. **85**, 693–722 (2011)
36. C.T. Wu, M. Koishi, Three-dimensional meshfree-enriched finite element formulation for micromechanical hyperelastic modeling of particulate rubber composites. Int. J. Numer. Methods Eng. **91**, 1137–1157 (2012)
37. I.T. Shvets, E.P. Dyban, Contact heat transfer between plane metal surfaces. Int. Chem. Eng. **12**, 621–624 (1964)
38. J.O. Hallquist, *LS-DYNA Theory Manual* (Livermore Software Technology Corporation, Troy, 2006)
39. B. Ren, C.T. Wu, E. Askari, A 3D discontinuous Galerkin finite element method with the bond-based peridynamics model for dynamics brittle failure analysis. Int. J. Impact Eng. **99**, 14–25 (2017)
40. P. Krasauskas, S. Kilikevičius, R. Česnavičius, D. Pačenga. Experimental analysis and numerical simulation of the stainless AISI 304 steel friction drilling process. Mechanika **20**, 590–595 (2014)
41. G.R. Johnson, W.H. Cook, A constitutive model and data for metals subjected to large strains, high strain rates, and high temperatures, in *Proceedings of the 7th International Symposium on Ballistics*, The Hague, 19–21 April 1983, pp. 541–547